A bonding and damage constitutive model for lightly cemented granular material

Doherty, James P.; Muir Wood, David

Published in:
Computers and Geotechnics

DOI:
10.1016/j.compgeo.2020.103732

Publication date:
2020

Computers and Geotechnics 127 (2020) 103732

Contents lists available at ScienceDirect

Computers and Geotechnics

journal homepage: www.elsevier.com/locate/compgeo

Research Paper

A bonding and damage constitutive model for lightly cemented granular material

James P. Doherty[a,*], David Muir Wood[a,b]

[a] School of Civil and Resource Engineering, The University of Western Australia, 35 Stirling Hwy, Crawley, WA 6009, Australia
[b] Division of Civil Engineering, Fulton Building, Dundee University, Dundee DD1 4HN, United Kingdom

ARTICLE INFO

Keywords:
Cement
Constitutive model
Soil
Hydration
Damage
Granular material

ABSTRACT

The behaviour of cemented granular material is complicated by the fact that the eventual cemented properties depend on the conditions under which cement hydration (curing) takes place. There are a number of situations in industry where granular materials are mixed with small quantities of cement and deployed in highly transient curing environments. Understanding and predicting the responses in these situations requires a constitutive model where cemented properties are an output, rather than a pre-determined input. This paper presents a constitutive model that is capable of representing the formation and destruction of bonding in weakly cemented granular material in a transient stress environment.

1. Introduction

Understanding the behaviour of cemented granular material is complicated by the fact that the eventual cemented properties depend on the conditions under which cement hydration (curing) takes place (Fahey et al., 2011; Cui and Fall, 2016b). In many practical situations, for example mine backfill; deep soil mixing (for ground improvement); and casings and plugs for offshore oil and gas production wells, these factors are transient and depend, in turn, on the mechanical properties of the material and how its properties evolve with time. Understanding and predicting the responses in these situations requires a constitutive model where cemented strength is an output, rather than a pre-determined input. The cemented strength output must capture the influence of curing conditions (e.g. effective stresses, void ratio and degree of saturation). The constitutive model must be suitable for implementation in a system model (finite element model) that is capable of representing complex boundary conditions. In this paper a constitutive model that accounts for curing stress history is presented.

The model developed in this project is particularly focused on applications to mine backfill, but may be equally applicable to other situations involving creation and degradation of lightly cemented granular material. The focus on mine backfill is motivated by the trend in mining practice to develop underground instead of open cut mines as the depth of available ore bodies increases. Underground mining operations create large voids known as stopes. Typical stopes might have plan dimensions of 10–30 m and heights up to 100 m. Backfilling stopes with a mixture of tailings (waste from ore processing) and cement (together forming cemented paste backfill, CPB), serves two purposes: it permits the mineral extraction from the rock left between the stopes; and it helps to ensure regional stability following extraction. Water is added to the cement-tailings mixture in order to achieve a slurry-like consistency so that the backfill material can be transported to the stope via a reticulation system. The cement content is usually low, for example 3–7 percent by mass, but the volumes are so large that the cost of cement may be as high as 25 percent of the overall cost of the mining operation. In fact, the cost of cement is often the largest ongoing operational cost item for underground mines, with large mines in Australia spending over $ 20 million per year (Grice, 2013). Therefore, a saving in cement proportion can have a significant economic benefit. Considering the carbon and energy associated with cement production, reducing the cement used by the mining industry will have a significant environmental benefit.

Backfilling operations often have a significant impact on the mining schedule, therefore stopes should be filled as quickly as possible. Prior to filling, barricades (or bulkheads) are constructed in access drives at stope bases to contain the backfill as it consolidates (under self-weight loading) from its initial slurry-like state. The stresses applied to the barricade depend primarily on the strength and deformation properties of the backfill during filling. Rapid filling can increase the risk of barricade failures because higher fill rates not only increase the self-weight excess pore pressures in the mine backfill, but also reduce the time period available for cement hydration to take place during filling

* Corresponding author.
E-mail addresses: james.doherty@uwa.edu.au (J.P. Doherty), d.muirwood@dundee.ac.uk (D. Muir Wood).

https://doi.org/10.1016/j.compgeo.2020.103732
Received 10 March 2020; Received in revised form 11 May 2020; Accepted 29 June 2020

(Thompson et al., 2012; Doherty et al., 2015; Cui and Fall, 2017). Barricade failures not only pose a serious risk to the safety of mine site personnel, but there are also significant economic consequences as a result of mine down time during the cleanup. Therefore, optimising the fill rate requires a very detailed understanding of the behaviour of mine backfill to manage these risks. Cement influences the strength of backfill in two ways. The most obvious contribution is through the formation of cemented bonds generating real cohesion as the cement hydrates. In addition, cement hydration results in chemical shrinkage (Helinski et al., 2007; Helinski et al., 2011) among others (Muir Wood and Doherty, 2014; Muir Wood et al., 2016; Walske and Doherty, 2017), which can be extremely effective at reducing pore pressures in low permeability fills. A reduction in pore pressure results in an increase in effective stress and therefore an increase in frictional strength and reduced pressure on structural barricades.

As mining progresses, faces of backfilled stopes may become exposed when adjacent stopes are mined. It is this configuration, (rather than the process of filling) that usually dictates the required strength and therefore cement content (Li, 2014). The cemented strength that is ultimately achieved for a given cement content is known to depend on the density and effective stress during hydration (Fahey et al., 2011). Therefore, a rational assessment of behaviour of exposed backfill requires an ability first to simulate the filling process in order to establish the state of the backfill to be used as a starting point for simulating the exposure.

Because the bonding in the cemented backfill is relatively weak, it can be readily damaged by subsequent deformation. The constitutive model described here thus combines the two processes: cement hydration leading to formation of bonds; and strain-induced damage which progressively removes the bonds.

Constitutive models have been developed to describe the behaviour of uncemented soils using the theory of hardening plasticity with additional components of kinematic hardening and bounding surface plasticity (Roscoe and Schofield, 1963; Dafalias, 1986; Dafalias and Herrmann, 1982). The volumetric hardening Cam clay models and their kinematic hardening extensions have proved rather satisfactory for describing the behaviour of normally consolidated and overconsolidated clays in which the very open pore space leads to significant volumetric compression which controls the plastic hardening. Sands and related granular materials develop irrecoverable deformations primarily by particle rearrangement. For these materials, distortional hardening extensions of the much used Mohr–Coulomb model have proved successful (Gajo and Muir Wood, 1999; Doherty and Muir Wood, 2012).

To model natural soils, which have structure and interparticle bonding, extra features are required. Effects of structure have been incorporated in extensions of the models for unbonded materials to produce models for weak rocks, which can describe the progressive breakage of the bonds by weathering or by plastic strains, and the eventual return to a material without bonding or structure (Nova et al., 2003; Rouainia and Muir Wood, 2000). These constitutive models are all static, in that they describe the mechanical response of geomaterials after all cementation has finished. In this situation, the cemented strength is a known, or at least a measurable property of the material, and these models are concerned with describing a progressive loss of strength through shear deformation.

Relatively simple Mohr–Coulomb constitutive models have been applied to simulate mine backfill problems, where the influence of cementation is accounted for by adjusting model parameters as a function of hydration time (Doherty, 2015; Doherty and Muir Wood, 2016; Helinski et al., 2011). More recently, Cui and Fall (2016a) have presented a Drucker-Prager elasto-plastic constitutive model where the properties vary as a function of the degree of hydration. In this model, the degree of hydration is influenced by time and curing temperature, but not curing stresses.

This paper presents a new constitutive model describing the formation and destruction of bonding in weakly cemented granular material, with particular application to mine backfill, that accounts for curing density in the formation and destruction of bonding as well as the evolution of critical state line.

2. Constitutive model for bonded/unbonded material

The material is assumed to have purely frictional strength in its original, pre-cemented, state and to return to a purely frictional condition when all cement bonds have been destroyed by plastic straining. In its unbonded state (at either extreme of its life history) the fill will be described by a model similar to Severn-Trent sand which is itself an extension of the very familiar Mohr-Coulomb model (Gajo and Muir Wood, 1999). This model (like most other recent models for granular materials) assumes that with continuing shear deformation the soil/fill will eventually reach an asymptotic *critical state* in which distortional strain can continue indefinitely without further change in stress, volume, particle size distribution or particle arrangement (on average). Such an asymptotic state may well be unattainable in conventional laboratory testing apparatus because of practical limitations on the shear distortions that can be imposed without jeopardising the uniformity of the sample. However, the mechanical properties of the fill are expected to be dependent on a *state parameter* which indicates the volume or density change needed to reach the critical state at the current stress level.

The model developed in this paper is formulated for triaxial stress conditions (Fig. 1). This simplifies the model derivation and implementation, but allows many aspects of material behaviour to be explored. In simulating triaxial response, it is necessary to choose appropriate work-conjugate pairs of stress and strain variables. These variables separate the volumetric and distortional (shear) effects. The volumetric response is described in terms of a mean effective stress $p' = (\sigma'_a + 2\sigma'_r)/3$ where σ'_a and σ'_r are the axial and radial effective stresses, respectively. The volumetric strain $\varepsilon_p = \varepsilon_a + 2\varepsilon_r$, where ε_a and ε_r are the axial and radial strains, respectively. The distortional (shear) response is described using the deviator stress $q = \sigma'_a - \sigma'_r$ and distortional strain $\varepsilon_q = 2(\varepsilon_a - \varepsilon_r)/3$.

We adopt a convention that lower case bold notation refers to vector quantities while upper case bold notation refers to matrix quantities so that a typical stiffness matrix $\boldsymbol{D}$ links incremental stress ($\delta\boldsymbol{\sigma} = [\delta p', \delta q]^T$) and strain ($\delta\boldsymbol{\varepsilon} = [\delta\varepsilon_p, \delta\varepsilon_q]^T$). Then for elastic behaviour

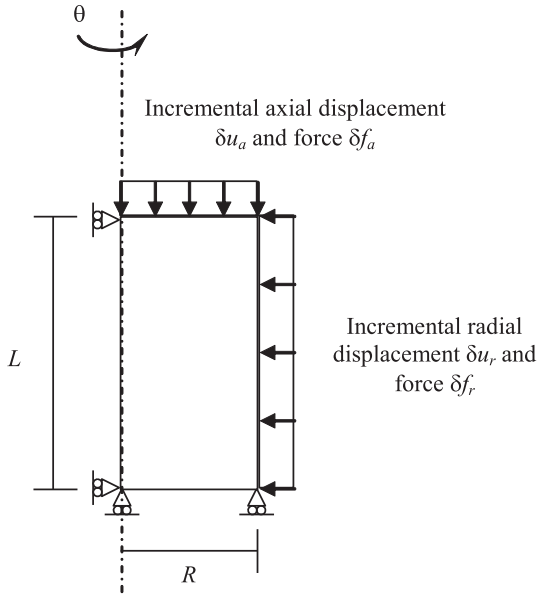

Fig. 1. Triaxial element boundary conditions.

$$\delta\boldsymbol{\sigma} = \boldsymbol{D}\delta\boldsymbol{\varepsilon} \tag{1}$$

where

$$\delta\boldsymbol{\sigma} = \begin{pmatrix} \delta p' \\ \delta q \end{pmatrix}, \delta\boldsymbol{\varepsilon} = \begin{pmatrix} \delta\varepsilon_p \\ \delta\varepsilon_q \end{pmatrix}, \boldsymbol{D} = \begin{bmatrix} K & 0 \\ 0 & 3G \end{bmatrix} \tag{2}$$

where K is the elastic bulk modulus and G is the elastic shear modulus.

3. Cemented strength: cohesion/attraction

It is assumed that cement hydration occurs at a steadily decreasing rate with time, so that the current degree of hydration is ζ

$$\zeta = 1 - \exp(-\kappa_h t_h) \tag{3}$$

where t_h is hydration time and κ_h is the rate of hydration parameter. As the cement hydrates, the material develops some real bonding which can be described by an attraction (a). The increase in attraction (δa^h) due to hydration during a time increment δt_h is

$$\delta a^h = a_f f(\sigma)\kappa_h \exp(-\kappa_h t_h)\delta t_h \tag{4}$$

where a_f is an indication of the maximum attraction that can be reached. A number of researchers (e.g. Fahey et al., 2011; Dalla Rosa et al., 2008) have demonstrated that the cemented strength of granular materials increases if they are cured under higher densities, or lower specific volumes. To account for this, the expression $f(\sigma)$ is included in Eq. (4) where

$$f(\sigma) = 1 + \lambda_a \left(\frac{\hat{v} - v}{\hat{v} - \check{v}} \right)^{m_a} \tag{5}$$

where v is the current specific volume that is tracked as a state parameter throughout the analysis. $\hat{v}$ and $\check{v}$ are model input parameters representing upper and lower limits on the specific volume. Parameters m_a and λ_a give the expression the flexibility to model a non-linear variation in cemented strength as function of specific volume. This expression implies that, in the absence of attraction damage (discussed in the following section), a sample cured at the upper bound specific volume achieves an attraction of 99 percent of its final strength (a_f) when $\kappa_h t_h = 5$ (see Fig. 2), whereas a sample cured at the lower bound specific volume will achieve a cemented strength of $a_f(\lambda_a + 1)$.

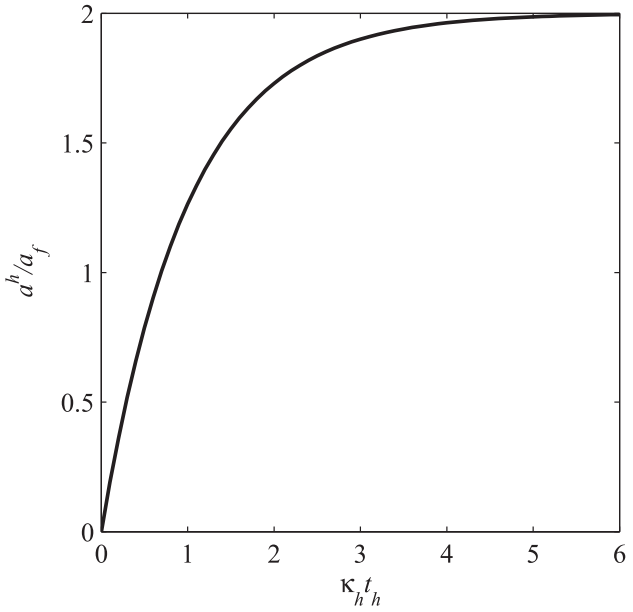

Fig. 2. The development with dimensionless hydration time of attraction normalised by input parameter a_f for material cured under $v = \hat{v}$.

4. Damage to strength

It has been shown that the cemented bonds formed during hydration can be destroyed by plastic strains (e.g. Fahey et al., 2011; Ghirian and Fall, 2014). To account for this, a damage strain increment ($\delta\varepsilon_d$) is defined as

$$\delta\varepsilon_d = \sqrt{\alpha(\delta\varepsilon_p^p)^2 + (1-\alpha)(\delta\varepsilon_q^p)^2} \tag{6}$$

The model parameter α is used to allow the relative significance of plastic volumetric strain ($\delta\varepsilon_p^p$) and plastic distortional strain ($\delta\varepsilon_q^p$) to be specified. Then the effect of the damage is defined as

$$\delta a^d = -a k_a \delta\varepsilon_d \tag{7}$$

where k_a is a model parameter defining the rate of destruction of cemented strength with damage strain. The actual "operating" cemented strength at any time in the model has now been defined as a function of two competing mechanisms; one increases the cemented strength with time due to hydration (Eq. (4)) and the other destroys it with plastic strain (Eq. (7)), so that

$$\delta a = \delta a^h + \delta a^d \tag{8}$$

It is evident that with continued plastic deformation the cemented strength will be entirely lost. This is appropriate for a model constructed within a framework of critical state soil mechanics.

5. Critical states and state parameter

For uncemented material it is common to assume that a critical state line can be defined in the compression plane, linking states for which continuing constant volume shearing occurs. A general form of the critical state line in the compression plane is

$$v_c = \check{v} + (\hat{v} - \check{v})\exp[-(p'/p'_v)^{m_v}] \tag{9}$$

where p'_v is a reference pressure and m_v is a model parameter that controls the shape of the critical state line. During cementation, cement combines with water to form a gel. This conversion of water into solids reduces the volume of the voids in the cementing material and, therefore, reduces the specific volume (v). This aspect of hydration may be difficult to capture directly, but the effect of this may be accounted for by adjusting the critical state line as a function of the present operational cemented strength and the degree of hydration. This may be achieved by modifying Eq. (9):

$$v_c = \check{v} + (\hat{v} - \check{v})\exp[-(p'/p'_v)^{m_v}] + k_{va}\frac{a}{2a_f} + k_{v\zeta}\zeta \tag{10}$$

where k_{va} and $k_{v\zeta}$ are model parameters. The ratio $a/2a_f$ and ζ are zero prior to hydration. As damage strain occurs, a reduces, and this reduces the impact of cementation on the critical state line. A state parameter can then be defined as a function of the current specific volume (v) and the specific volume on the operating critical state line at an equivalent mean effective stress

$$\psi = v - v_c \tag{11}$$

6. Elasticity

A hypoelastic model is assumed in which the bulk stiffness (K) is related to the mean effective stress (p') and the current cemented strength (a).

$$K = K_{ref}\left(\frac{p' + a}{p'_K}\right)^{m_K} \tag{12}$$

where m_K (exponent) and p'_K (reference pressure) are model parameters. This accommodates the idea that, as plastic shearing damages the bonding, both the stiffness and the strength will fall together. The shear stiffness is calculated based on a constant Poisson's ratio μ

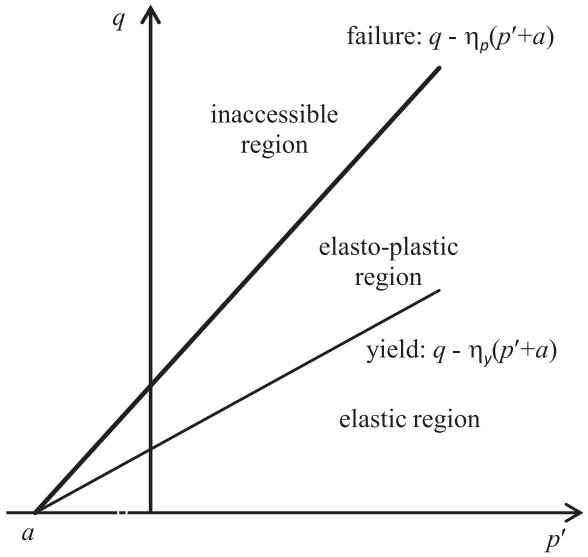

Fig. 3. The Extended Mohr-Coulomb soil model with yield locus separating elastic and elasto-plastic regions and a failure locus separating elasto-plastic and inaccessible regions.

$$G = \frac{3(1-2\mu)}{2(1+\mu)}K \tag{13}$$

7. Yield surface

The yield surface in p': q stress space is assumed to be

$$F = q - \eta_y(p' + a) = 0 \tag{14}$$

where η_y is a hardening parameter defining the slope of the current yield surface and a is the current attraction, which defines the cemented components of strength (Fig. 3). The slope of the yield surface in the p': q plane can be related to a Mohr–Coulomb mobilised friction angle (ϕ_y) via

$$\sin\phi_y = \frac{3\eta_y}{\eta_y + 6} \tag{15}$$

Expressing the cemented strength as an attraction (a) rather than the more typical cohesion (c) is done purely to simplify the mathematical derivation of the model. However, attraction and cohesion can be related as $c = a\tan\phi_y$. In the following sections of the paper, expressions for the increase in cemented strength due to hydration time (δa^h) and a reduction of cemented strength due to plastic damage strains (δa^d) are introduced. A hardening rule is also defined that allows η_y to expand up to a limiting failure locus, defined by η_p (see Fig. 3).

8. Shear hardening

The aim of this model is to describe a mechanical response in which the stiffness of the material steadily falls as it is sheared towards failure, similar to the Severn Trent Sand Model (Gajo and Muir Wood, 1999) and the Extended Mohr Coulomb model (Doherty and Muir Wood, 2012). This can be achieved by introducing a simple relationship between plastic distortional strain and mobilised shear stress, in which the plastic distortional strain increases exponentially (towards infinity) as η_y approaches the peak frictional strength η_p

$$\varepsilon_q^p = \frac{\beta\eta_y}{\eta_p - \eta_y} - \frac{\beta\eta_y^0}{\eta_p - \eta_y^0} \tag{16}$$

where β is a model input parameter and η_y^0 is the maximum previously mobilised shear stress defined when establishing the initial conditions. This is used in Eq. (16) to ensure that the plastic shear strain is zero when the initial yield surface (defined using η_y^0) is first encountered (i.e. $\eta_y = \eta_y^0$). It should be noted that when $\eta_y \leqslant \eta_y^0$ the model remains elastic and Eq. (16) is not invoked. It is then convenient to introduce the constant

$$\xi = \frac{\eta_y^0}{\eta_p - \eta_y^0} \tag{17}$$

as it can be shown that $\varepsilon_q^p = \beta$ when

$$\frac{\eta_y}{\eta_p} = \frac{1+\xi}{2+\xi} \tag{18}$$

This implies, for example, that a sample that has only ever experienced isotropic stress conditions, with $\eta_y^0 = 0$ (giving $\xi = 0$) will develop a plastic shear strain of β when 50% of the available frictional strength is mobilised.

For implementation in an elasto-plastic framework, the rate of change of the hardening parameter with respect to the plastic distortional strain is required. It can be shown that

$$\frac{\delta\eta_y}{\delta\varepsilon_q^p} = \frac{(\eta_p - \eta_y)^2}{\beta\eta_p} \tag{19}$$

The frictional strength of granular materials depends on their density and on the effective stress level. The state parameter ψ combines both these variables (density through v and stress level through v_c). We assume that the current peak strength of the material, η_p, is not constant but depends on state parameter according to a linear relationship such as:

$$\eta_p = \eta_{cv}\max(1, (1 - k_p\psi)) \tag{20}$$

9. Dilatancy

This state parameter can then be used to define the ratio of incremental plastic volumetric and shear strains

$$\frac{\delta\varepsilon_p^p}{\delta\varepsilon_q^p} = k_d\psi + (\eta_{cv} - \eta_y) - \frac{a}{a_f}\eta_y \tag{21}$$

where k_d is a model parameter that defines the influence of the state parameter; and η_{cv} is a mobilised friction at which constant volume shearing takes place.

10. Model summary

A shear hardening, cement bonding and damage model has now been defined that captures many important features of cementing mine backfill. The complete list of model parameters is given in Table 1. In addition to these parameters the initial conditions must be defined: stress state, specific volume and maximum previously mobilised friction. The mobilised friction η_y and the available cemented strength a are both solution dependent variables. Changes in the specific volume

Table 1
Model parameters.

Model Parameter	Description	Value	Equation
Elastic parameters			
K_{ref}	reference bulk stiffness	50 MPa	12
p'_K	reference pressure	100 kPa	12
m_K	exponent	0.8	12
μ	Poisson's ratio	0.2	13
Critical state line			
$\hat{v}$	maximum specific volume	1.72	9
$\dot{v}$	minimum specific volume	1.5	9
p'_v	reference pressure	500 kPa	9
m_v	exponent	1	9
k_{va}	influence of attraction	0.05	9
$k_{v\zeta}$	influence of attraction	0.25	9
Frictional strength			
η_{cv}	critical state strength	1.3	20
k_p	influence of state on strength	1.2	20
Shear hardening			
β	strain scaling	0.01	16
Dilatancy			
k_d	influence of state	3.5	21
Cementation			
κ_h	rate of hydration	0.007 h^{-1}	4
a_f	limiting attraction	700 kPa	4
m_a	attraction exponent	1	4
λ_a	attraction coefficient	1	4
α	damage divider	0.5	6
k_a	damage coefficient	25	5

due to volumetric strains are tracked so the current specific volume can be used to calculate the state parameter ψ from Eq. (11) and cemented strength gain from Eq. (5).

It may seem excessively complicated to define a 20 parameter model for a cementing granular material. One reason for the large number of parameters is that, to date, few test data of the kind needed to verify the detailed behaviour of cementing granular materials have been available. Therefore, the model has been defined in very general terms. As experience is gained in applying the model, it is expected that a number of parameters may be removed. It should also be noted that, unlike materials geotechnical engineers usually encounter, mine backfill is not naturally occurring. It is an engineered product that can be produced consistently over many years and is therefore not subject to the same variability that naturally occurring materials typically exhibit. Therefore, the investment in extensive laboratory testing program to adequately define the mechanical behaviour may be justified.

11. Comparison of model response with published data

The model was implemented as outlined in Appendix 1 and applied to simulate a series of triaxial compression tests reported by Dalla Rosa et al., 2008. These tests involved curing samples with 3 percent Portland cement for 48 h at isotropic confining pressures of 50, 250 and 500 kPa. The curing stresses of 50, 250 and 500 kPa corresponded to curing specific volumes of 1.624, 1.573 and 1.535 respectively, giving rise to differences in cemented strengths. Drained triaxial compression tests were then carried out from initial isotropic confining pressures of 50, 250 and 500 kPa. Uncemented samples were also tested at each of the confining pressures.

To match the data, the model was first tuned to match the uncemented isotropically consolidated triaxial compression tests at each confining pressure. Parameters that impact the cemented response of the model were then adjusted to match the cemented tests at a confining pressure of 250 kPa. The parameters were then kept constant and the model applied to simulate tests with confining pressures of 50 kPa and 500 kPa. The shear stress–strain and volumetric-shear strain results are presented in Fig. 4. The parameters used for all simulations are given in Table 1.

It can be seen from Fig. 4b that the model provides a good match to the test data with a confining pressure of 250 kPa (i.e. the test data used in the calibration process). The peak strength and the rate of softening as a result of damage to the cemented bonds are well captured. The volumetric response is also reasonably well matched, although the sample cured at 50 kPa shows significant dilation after a shear strain of around 0.07, compared with the model.

The response of the model in the compression plane for all tests at 250 kPa is presented in Fig. 5. This figure shows the initial critical state line (CSL), which is the same for all samples (this is independent of cementation). After curing for 48 h at a given confining stress, the CSL moves up as a function of both the degree of hydration and the cemented attraction that has developed. Because the attraction varies with curing density (or specific volume), the CSL at the end of curing varies among tests. At the end of shearing, the attraction is almost completely destroyed and the CSL moves down. However, it does not move back to the uncemented CSL due to the conversion of water into solids as a result of the hydration process. The cemented samples end up in a very similar position in terms of specific volume and stress, which is in keeping with the notion of a critical state damage model. The uncemented sample, which is fundamentally a different material, ends in a very different position.

With the parameters derived to match the tests with a confining pressure of 250 kPa, the model was then used to predict the response of tests with confining pressures of 50 kPa and 500 kPa. It can be seen from Fig. 4a and 4c that the model provided a reasonable match to the data, although not as good as it does for the calibration data (Fig. 4b).

For the tests with a confining pressure of 50 kPa (Fig. 4a), the model provides a reasonable match to the cemented strength for the samples cured at 50 kPa and 250 kPa. However, for samples cured at 500 kPa, the model overestimates the cemented strength. This may be because isotropic unloading damages bonds due to volumetric strain. The model presented in this paper does not include a cap and therefore cannot account for damage induced purely by changes in mean effective stress. The volumetric response (Fig. 4a) is reasonably well captured, with the model bounding the measured response. The stress path in the compression plane for all tests with a confining pressure of 50 kPa is presented in Fig. 6. The cemented samples end up in a similar position, in keeping with a critical state model.

For the tests with a confining pressure of 500 kPa (Fig. 4c), the model under predicts the cemented strength. In the compression plane, the model tends to under predict the initial contraction, but over predicts the contraction at higher strains. The over prediction at higher

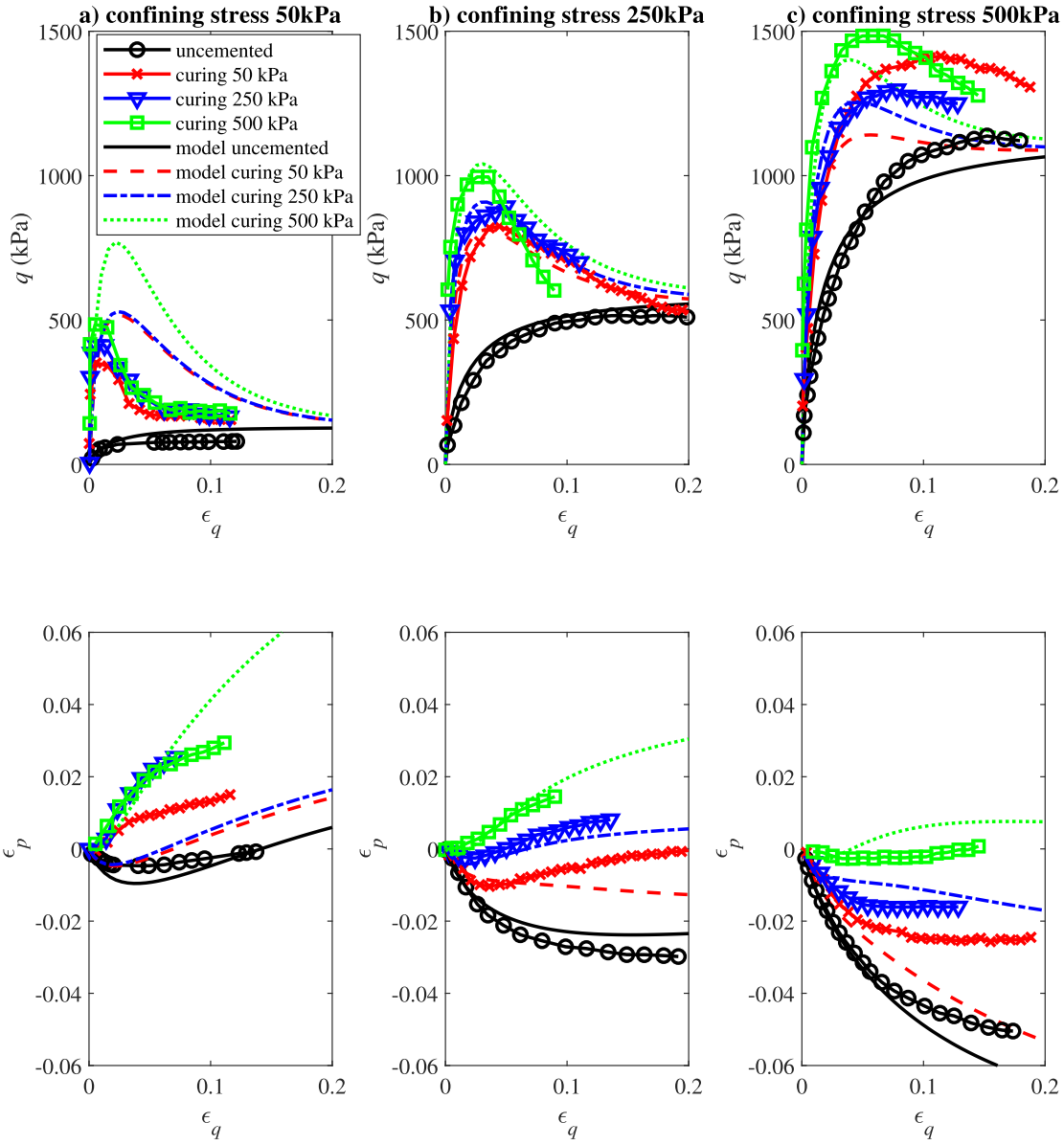

Fig. 4. Stress–strain response and volumetric behaviour of measured data versus model response (a) confining stress of 50 kPa; (b) confining stress of 250 kPa, (c) confining stress of 500 kPa.

strains may indicate the movement of the CSL should be lower. The compression response is illustrated in Fig. 7, again illustrating the tendency for the model to arrive at similar stress and density despite different stress and curing history.

12. Discussion

Our intention has been to demonstrate how a hydration model of strength gain can be combined with a fairly simple constitutive model for an uncemented soil or soil_like material in order to show the interaction of time-dependent evolution of a modest bond strength (cement hydration) with a rate-independent soil. The model has been presented in a modular fashion - elasticity, yield, dilatancy, hardening, critical states, - so that the need for all the soil parameters can be recognised. (As a rule of thumb each new nonlinear effect requires an extra 2 parameters for its description.) The modular approach also makes clear how one might introduce alternative functions to describe each module of behaviour. For example, the critical state line is often

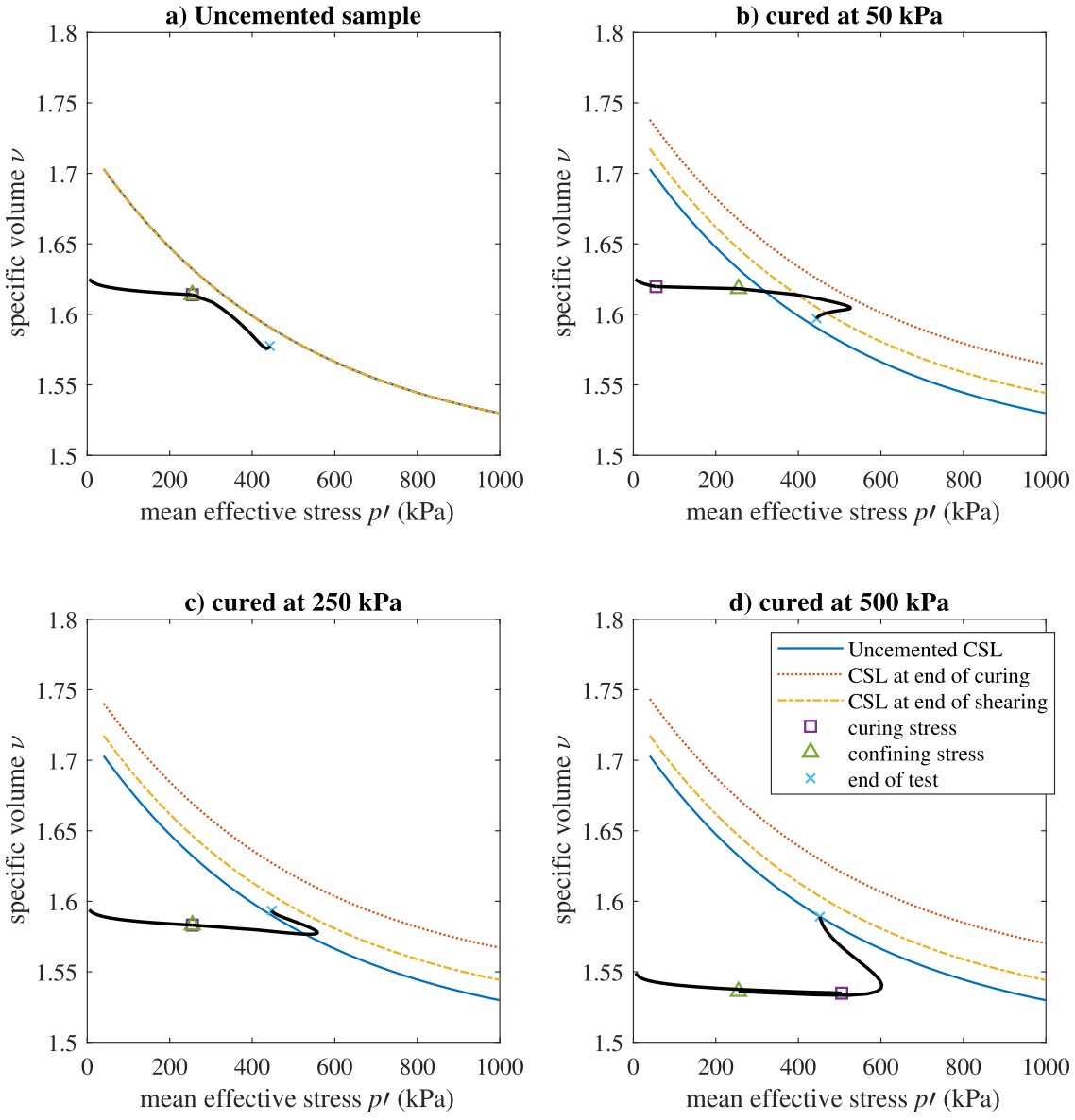

Fig. 5. compression plane for tests with a confining pressure of 250 kPa, with (a) no cement, (b) curing stress of 50 kPa (c) curing stress of 250 kPa (d) curing stress of 500 kPa.

described using a semi-logarithmic form, $v_c = \Gamma - \lambda \ln p'$. But this function tends to $\pm \infty$ for vanishingly small or extremely large values of mean stress p'. This may not matter if we are confident that our stresses will remain in a stable middle range - and we could save some soil parameters in the process. Similarly, we have assumed that it is the specific volume at each time during hydration that contributes to the eventual nature of the bond strength. It might be anticipated that curing under a non-isotropic effective stress state would lead to a correspondingly anisotropic increment of bond strength. This change can be readily made to the bonding module. The dominant element of the flow rule is the dependence of the dilatancy on the current stress ratio $\eta = q/p'$ relative to the critical state stress ratio. This feature is very evident in Figs. 4a, b, c. The current slope of the incremental volumetric strain relationship in the lower diagram of each pair is controlled primarily by the value of stress ratio in the upper diagram with some allowance included for the current values of state parameter ψ and of strength represented by the attraction a. Both state parameter and strength tend to zero as the critical state is approached. The model was calibrated to match the behaviour of the uncemented material over a range of stress levels. Parameters impacting cementation were then

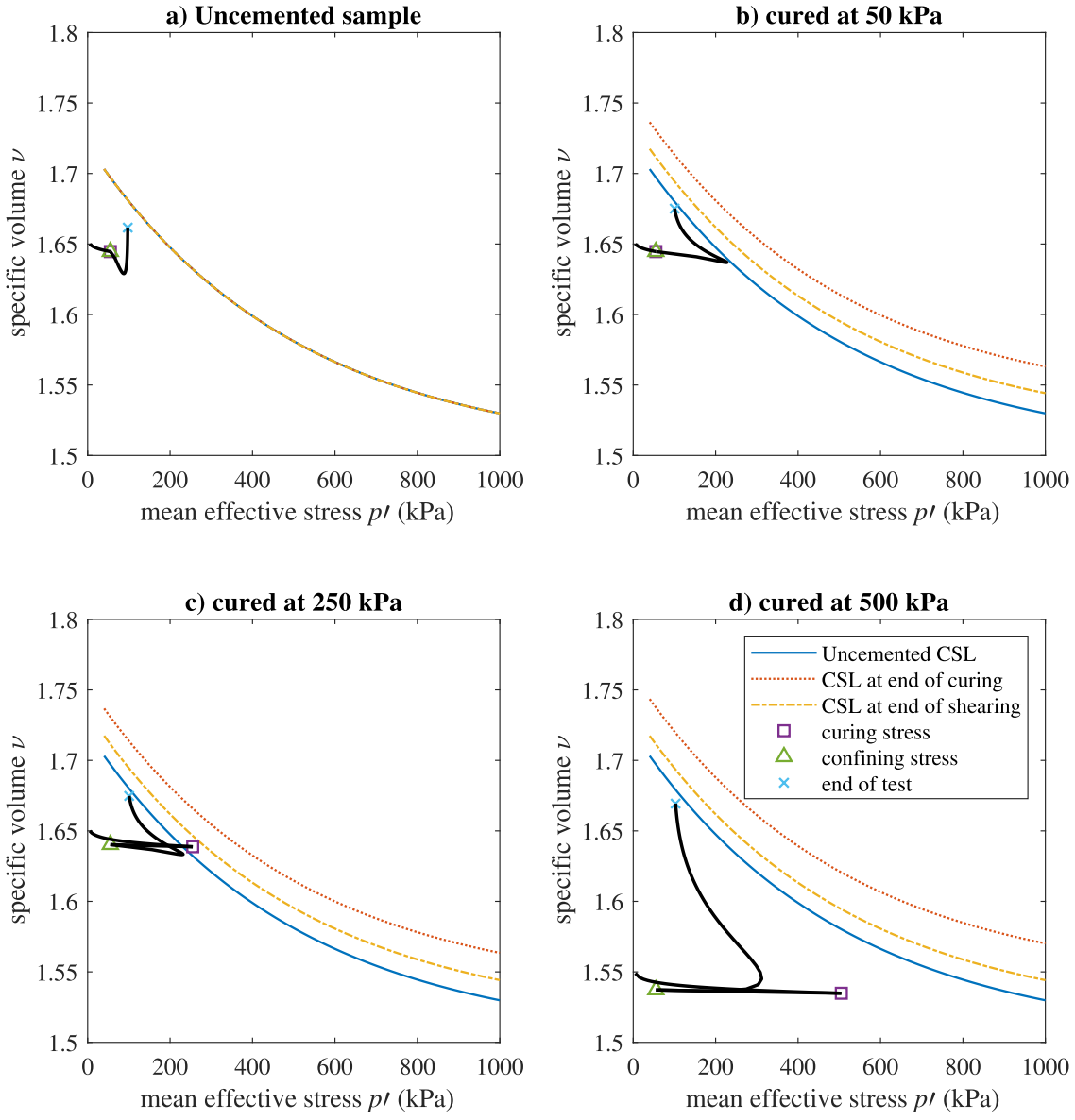

Fig. 6. Compression plane for tests with a confining pressure of 50 kPa, with (a) no cement, (b) curing stress of 50 kPa (c) curing stress of 250 kPa (d) curing stress of 500 kPa.

calibrated to match data for a confining stress of 250 kPa and a good agreement with the data was achieved. The model was then applied to predict the cemented behaviour of tests at confining stresses of 50 and 500 kPa. It was found that the model over predicted the strength of samples that were cured under high stress and sheared under lower stresses. This may indicate the need for additional features in the model, such as a cap that could allow for plastic deformation during isotropic unloading.

13. Conclusions

A modular framework has been described for the development of a constitutive model which combines creation and elimination of inter-particle bonding. The particular model for the bonding-free soil is Severn-Trent sand - a frictional hardening material for which many aspects of response are controlled by the proximity to a critical state line. The steady elimination of interparticle bonding with continuing straining in the present model ensures that the existence of critical

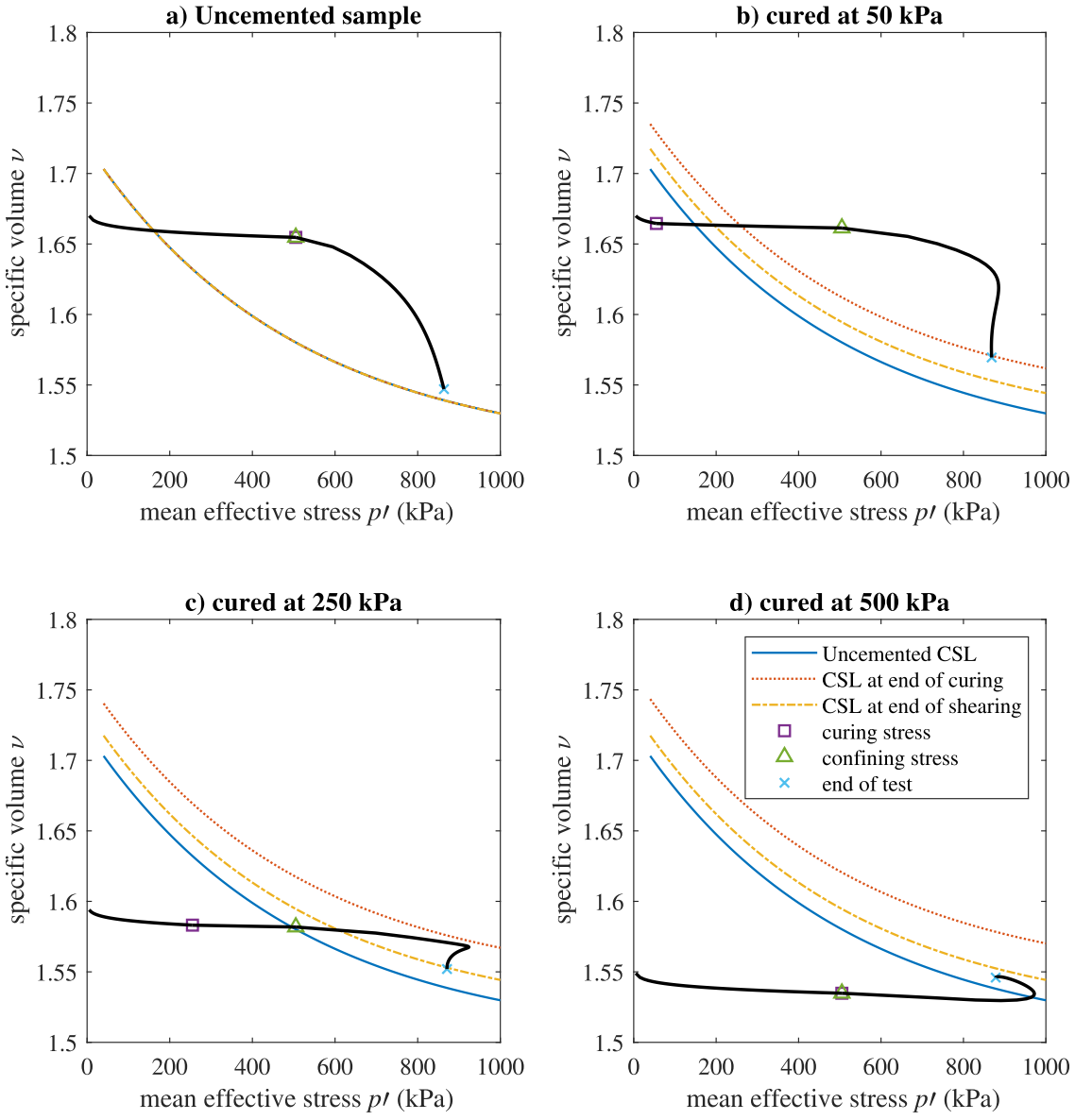

Fig. 7. Compression plane for tests with a confining pressure of 500 kPa, with (a) no cement, (b) curing stress of 50 kPa (c) curing stress of 250 kPa (d) curing stress of 500 kPa.

states is preserved. The rate at which interparticle bonding is built up is controlled by the dimensionless product $\kappa_h t_h$ in Eq. (3). In our present simulations $\kappa_h = 0.007h^{-1}$ indicating a time of 140 h to full hydration. But we could use the same procedure, with a much lower value of κ_h to model geological processes by which deposits from silicate or carbonate loaded pore fluid gradually generate interparticle bonding. The modules of the model remain the same.

Declaration of Competing Interest

The authors declare that they have no known competing financial interests or personal relationships that could have appeared to influence the work reported in this paper.

Appendix A. Model implementation

In elasto-plasticity, strain increments can be split into elastic $\delta\varepsilon^e$ and plastic $\delta\boldsymbol{\varepsilon}^{\mathbf{p}}$ components

$$\delta\varepsilon = \delta\varepsilon^e + \delta\varepsilon^p \tag{22}$$

where $\delta\epsilon$ is the total strain increment. The incremental stress $\delta\sigma$ is related to the elastic strain increment through the elastic constitutive matrix $\boldsymbol{D}$

$$\delta\sigma = \boldsymbol{D}\delta\varepsilon^e \tag{23}$$

The direction of the plastic strains is determined by the gradient to the plastic potential at the current stress and the magnitude of plastic strains are determined by the plastic multiplier Λ, such that

$$\delta\varepsilon^p = \Lambda\frac{\partial Q}{\partial\sigma} \tag{24}$$

Combining Eqs. (22)–(24) gives the following expression for incremental stress in terms of total strain

$$\delta\boldsymbol{\sigma} = \boldsymbol{D}\delta\boldsymbol{\varepsilon} - \Lambda\boldsymbol{D}\frac{\partial Q}{\partial \boldsymbol{\sigma}} \tag{25}$$

Noting that the yield surface can move due shear hardening ($\delta\eta_y$), damage to the cemented bonds due to plastic strain (δa^d) and cement hydration (δa^h) over time, the consistency condition requires that

$$\frac{\partial F}{\partial \boldsymbol{\sigma}}^T \delta\boldsymbol{\sigma} + \frac{\partial F}{\partial \eta_y}\delta\eta_y + \frac{\partial F}{\partial a}\delta a^d + \frac{\partial F}{\partial t}\delta t = 0 \tag{26}$$

which can be expanded and written as

$$\frac{\partial F}{\partial \boldsymbol{\sigma}}^T \delta\boldsymbol{\sigma} + \frac{\partial F}{\partial \eta_y}\delta\eta_y + \frac{\partial F}{\partial a}\delta a^d + \frac{\partial F}{\partial a}\frac{\partial a^h}{\partial t}\delta t = 0 \tag{27}$$

From Eqs. (22)–(24)

$$\frac{\partial F}{\partial \boldsymbol{\sigma}}^T \delta\boldsymbol{\sigma} = \frac{\partial F}{\partial \boldsymbol{\sigma}}^T \boldsymbol{D}\delta\boldsymbol{\varepsilon} - \Lambda\frac{\partial F}{\partial \boldsymbol{\sigma}}^T \boldsymbol{D}\frac{\partial Q}{\partial \boldsymbol{\sigma}} \tag{28}$$

Combining Eqs. (28) and (27) gives

$$\frac{\partial F}{\partial \boldsymbol{\sigma}}^T \boldsymbol{D}\delta\boldsymbol{\varepsilon} - \Lambda\frac{\partial F}{\partial \boldsymbol{\sigma}}^T \boldsymbol{D}\frac{\partial Q}{\partial \boldsymbol{\sigma}} + \frac{\partial F}{\partial \eta_y}\delta\eta_y + \frac{\partial F}{\partial a}\delta a^d + \frac{\partial F}{\partial a}\frac{\partial a^h}{\partial t}\delta t = 0 \tag{29}$$

and it can be shown that the plastic multiplier is then given by

$$\Lambda = \frac{\frac{\partial F}{\partial \boldsymbol{\sigma}}^T \boldsymbol{D}\delta\boldsymbol{\varepsilon} + \frac{\partial F}{\partial a}\frac{\partial a^h}{\partial t}\delta t}{\frac{\partial F}{\partial \boldsymbol{\sigma}}^T \boldsymbol{D}\frac{\partial Q}{\partial \boldsymbol{\sigma}} + H} \tag{30}$$

where

$$H = -\frac{1}{\Lambda}\left(\frac{\partial F}{\partial \eta_y}\delta\eta_y + \frac{\partial F}{\partial a}\delta a^d\right) \tag{31}$$

From Eqs. (28) and (27)

$$\frac{\partial F}{\partial \eta_y} = -(p + a) \tag{32}$$

$$\frac{\partial F}{\partial a} = -\eta_y \tag{33}$$

and

$$\frac{\partial F}{\partial \boldsymbol{\sigma}} = \begin{pmatrix} \frac{\partial F}{\partial p'} \\ \frac{\partial F}{\partial q} \end{pmatrix} = \begin{pmatrix} -\eta_y \\ 1 \end{pmatrix} \tag{34}$$

From Eq. (21)

$$\frac{\partial Q}{\partial \boldsymbol{\sigma}} = \begin{pmatrix} \frac{\partial Q}{\partial p'} \\ \frac{\partial Q}{\partial q} \end{pmatrix} = \begin{pmatrix} (1 - \frac{a}{a_{max}}\zeta)(\eta_{cv} - \eta_y) - \frac{a}{a_{max}}\zeta\eta_y\frac{\hat{v} - v}{\hat{v} - \tilde{v}} \\ 1 \end{pmatrix} \tag{35}$$

$\delta\eta_y$ (from Eq. (19)) can now be expressed in terms of Λ

$$\delta\eta_y = \frac{(\eta_p - \eta_y)^2}{\beta\eta_p}\Lambda\frac{\partial Q}{\partial q} = \frac{(\eta_p - \eta_y)^2}{\beta\eta_p}\Lambda \tag{36}$$

An expression for the damage strain can also be obtained in terms of Λ

$$\delta a^d = -ak_a\Lambda\sqrt{\alpha\left(\frac{\partial Q}{\partial p'}\right)^2 + (1 - \alpha)\left(\frac{\partial Q}{\partial q}\right)^2} \tag{37}$$

Substituting Eqs. (36) and (37) into Eq. (31) gives H independent of Λ.

$$H = (p + a)\frac{(\eta_p - \eta_y)^2}{\beta\eta_p} - \eta_y ak_a\sqrt{\alpha\left(\frac{\partial Q}{\partial p'}\right)^2 + (1 - \alpha)\left(\frac{\partial Q}{\partial q}\right)^2} \tag{38}$$

With this expression for H, Λ can be found from Eq. (30). The hardening parameter η_y is updated according to Eq. (36) and the attraction parameter is updated using

$$\delta a = \delta a^h + \delta a^d \tag{39}$$

where δa^h comes from Eq. (4) and δa^d comes from Eq. (37).

References

Cui, L., Fall, M., 2016a. An evolutive elasto-plastic model for cemented paste backfill. Comput. Geotech. 71 (Supplement C), 19–29.

Cui, L., Fall, M., 2016b. Mechanical and thermal properties of cemented tailings materials at early ages: Influence of initial temperature curing stress and drainage conditions. Constr. Build. Mater. 125 (Supplement C), 553–563.

Cui, L., Fall, M., 2017. Multiphysics modeling of arching effects in fill mass. Geotechnics 83, 114–131.

Dafalias, Y.F., 1986. Bounding surface plasticity. i: mathematical foundation and hypo-plasticity. J. Eng. Mech. ASCE 112.

Dafalias, Y.F., Herrmann, L., 1982. Bounding surface formulation of soil plasticity. In: Pande, G.N., Zienkiewicz, O.C. (Eds.), Soil Mechanics-transient and Cyclic Loads. Wiley, New York.

Dalla Rosa, F., Consoli, N.C., Baudet, B.A., 2008. An experimental investigation of the behaviour of artificially cemented soil cured under stress. Géotechnique 58, 675–679.

Doherty, J.P., 2015. A numerical study into factors affecting stress and pore pressure in free draining mine stopes. Comput. Geotech. 63, 331–341.

Doherty, J.P., Hasan, A., Suazo, G.H., Fourie, A., 2015. Investigation of some controllable factors that impact the stress state in cemented paste backfill. Can. Geotech. J. 52 (12), 1901–1912.

Doherty, J.P., Muir Wood, D., 2012. An extended mohr-coulomb (emc) model for predicting the settlement of shallow foundations on sand. Geotechnique 63, 661–673.

Doherty, J.P., Muir Wood, David, 2016. Back analysis of the kanowna belle stope filling case history. Comput. Geotech. 76, 201–211.

Fahey, M., Helinski, M., Fourie, A., 2011. Development of specimen curing procedures that account for the influence of effective stress during curing on the strength of cemented mine backfill. Geotech. Geol. Eng. 29 (5), 709–723.

Gajo, A., Muir Wood, D., 1999. Severn-trent sand: a kinematic-hardening constitutive model: the q-p formulation. Geotechnique 49, 595–614.

Ghirian, A., Fall, M., 2014. Coupled thermo-hydro-mechanical-chemical behaviour of cemented paste backfill in column experiments: Part ii: Mechanical, chemical and microstructural processes and characteristics. Eng. Geol. 170 (Supplement C), 11–23.

Grice, T., 2013. Mine backfill- a cost centre or an optimisation opportunity? Newsletter 41. Australian Centre for Geomechanics.

Helinski, M., Fahey, M., Fourie, A., 2011. Behavior of cemented paste backfill in two mine stopes: measurements and modeling. J. Geotech. Geoenviron. Eng. 137 (2), 171–182.

Helinski, M., Fourie, A., Fahey, M., Ismail, M., 2007. Assessment of the self-desiccation process in cemented mine backfills. Can. Geotech. J. 44 (10), 1148–1156.

Li, L., 2014. Analytical solution for determining the required strength of a side-exposed mine backfill containing a plug. Can. Geotech. J. 51 (5), 508–519.

Muir Wood, D., Doherty, J.P., 2014. Coupled chemical shrinkage and consolidation: Some benchmark solutions. Transp. Porous Media 105 (2), 349–370.

Muir Wood, D., Doherty, J.P., Walske, M.L., 2016. Deposition and self-weight consolidation of a shrinking fill. Géotechnique Lett. 6 (1), 72–76.

Nova, R., Castellanza, R., Tamagnini, C., 2003. A constitutive model for bonded geo-materials subject to mechanical and/or chemical degradation. Int. J. Numer. Anal. Meth. Geomech. 27, 705–732.

Roscoe, K.H., Schofield, A.N., 1963. Mechanical behaviour of an idealised 'wet' clay. Proc. European Conf. on Soil Mechanics and Foundation Engineering, Wiesbaden.

Rouainia, M., Muir Wood, D., 2000. A kinematic hardening constitutive model for natural clays with loss of structure. Geotechnique 112, 153–164.

Thompson, B.D., Bawden, W.F., Grabinsky, M.W., 2012. In situ measurements of cemented paste backfill at the cayeli mine. Can. Geotech. J. 49 (7), 755–772.

Walske, M.L., Doherty, J.P., 2017. Incorporating chemical shrinkage volume into gibson's solution. Can. Geotech. J.(ja).